Downloaded from orbit.dtu.dk on: Mar 29, 2019

DTU Library

Hybridization-induced dual-band tunable graphene metamaterials for sensing

Gong, Shaokang; Xiao, Binggang; Xiao, Lihua; Tong, Shengjun; Xiao, Sanshui ; Wang, Xiumin

Published in:
Optical Materials Express

Link to article, DOI:
10.1364/OME.9.000035

Publication date:
2019

Document Version
Publisher's PDF, also known as Version of record

Link back to DTU Orbit

Citation (APA):
Gong, S., Xiao, B., Xiao, L., Tong, S., Xiao, S., & Wang, X. (2019). Hybridization-induced dual-band tunable graphene metamaterials for sensing. Optical Materials Express, 9(1), 35-43. DOI: 10.1364/OME.9.000035

General rights
Copyright and moral rights for the publications made accessible in the public portal are retained by the authors and/or other copyright owners and it is a condition of accessing publications that users recognise and abide by the legal requirements associated with these rights.

- Users may download and print one copy of any publication from the public portal for the purpose of private study or research.
- You may not further distribute the material or use it for any profit-making activity or commercial gain
- You may freely distribute the URL identifying the publication in the public portal

If you believe that this document breaches copyright please contact us providing details, and we will remove access to the work immediately and investigate your claim.

Research Article | Vol. 9, No. 1 | 1 Jan 2019 | OPTICAL MATERIALS EXPRESS 35
Optical Materials EXPRESS

Hybridization-induced dual-band tunable graphene metamaterials for sensing

SHAOKANG GONG,[1] BINGGANG XIAO,[1,*] LIHUA XIAO,[2] SHENGJUN TONG,[1] SANSHUI XIAO,[3] AND XIUMIN WANG[1]

[1]College of Information Engineering, China Jiliang University, Hangzhou, 310018, China
[2]College of Chemical Engineering, Zhejiang University of Technology, Hangzhou, 310014, China
[3]Department of Photonics Engineering, Technical University of Denmark, Lyngby DK-2800, Denmark
[*]bgxiao@cjlu.edu.cn

Abstract: The infrared absorption spectrum due to structural vibrations in molecules has been widely used to resolve chemical identification. However, this method is limited by the weak molecule-light interaction. Graphene plasmon, having strong confinement and large field enhancement, provides a promising way to increase their interactions. Here we propose tunable hybridization-induced graphene nanostructures for sensing application. Our results reveal that when the symmetry of the graphene disk is broken by introducing a small circular defect, dual-band resonance can be excited at mid-infrared frequencies. The dual-band resonance peaks are produced by plasmon hybridization effect between two simple structures: graphene disks and circular defects. We investigate the influence of the size and position of the circular defect on the dual-band resonance peaks. We further explore the dual-band resonance peaks for sensing, and the sensitivity can reach 550 cm^{-1}/RIU and the FOM can reach 20.4. Compared to the original graphene disk structure, the results show stronger resonance intensity and higher frequency sensitivity. Our findings provide a new platform for sensing, and moreover the dual-band resonance structure feature enables us to promote the development of multi-substance detection.

© 2018 Optical Society of America under the terms of the OSA Open Access Publishing Agreement

1. Introduction

Plasmons, the collective oscillation of free electron in metal or doped graphene, have shown strong field confinement and large field enhancement, which giving us a unique platform to realize subwavelength nanoscale devices and sensing applications [1]. This appealing optical phenomenon has played an important role in filters, sensors, modulators, integrated functional components and so on [2–5]. In particular, the surface plasmon is very sensitive to the surrounding refractive index, and the resonance of the surface plasmon can be changed dramatic with a slight change in the refractive index of the sensing medium. Therefore, SPP-based sensors have attracted a lot of interests due to the reliability and high sensitivity of plasmon technology [6,7].

Traditional SPPs are based on noble metals and can only be excited at visible frequencies. This limits their application in the sensing field. In order to extend the operation range of the SPP and cover the frequency range from infrared to terahertz, metasurface and metamaterials have been proposed [8,9]. So far, various sensors based on metamaterials and metasurface have been proposed and studied [9–11]. However, surface plasmon sensors composed by conventional materials have a common drawback: once the structure is manufactured, the resonant wavelength of the sensor is fixed.

Fortunately, a new type of two-dimensional material, graphene, has attracted wide attention due to its excellent optical and electronic properties, such as high electron mobility and adjustable surface conductivity [12–15]. Compared with other traditional plasmonic materials, graphene-based devices have the advantages of low loss, long transmission length, and adjustable conductivity. The graphene device can change the resonant wavelength of the

#347858 https://doi.org/10.1364/OME.9.000035
Journal © 2019 Received 9 Oct 2018; revised 24 Oct 2018; accepted 25 Oct 2018; published 4 Dec 2018

Optical Materials EXPRESS

device by changing the chemical potential of the graphene instead of recreating the device [16,17]. In recent years, many graphene-based devices including sensors have been proposed and studied [18–23]. But the sensitivity of these sensors is yet to be improved. In addition, graphene surface plasmon sensors based on dual-band or multi-band also have great potential, but there are few studies in this area [24,25].

Here we propose a novel tunable hybridization-induced graphene nanostructure to achieve the dynamically tunable dual-band resonances in mid-infrared regions. When small circular defect was introduced in the graphene disk, the dual-band resonance peaks can be generated by plasmon hybridization between them. The excited dual-band resonance has polarization sensitivity and can be adjusted by controlling the position of the circular defect on the graphene disk. In addition, the responses spectral curves of the proposed graphene structure can be tuned by altering the Fermi level. The excited dual-band resonance peaks have superior refractive-index sensing performance. Thus, graphene metamaterials with tunable dual-band resonance peaks can exhibit potential applications in sensors and will help promote the development of multi-substance detection.

2. Results and discussion

2.1 Structural design and physical mechanism

Figures 1(a) and 1(b) display a segment of the proposed structure, consisting of an array of graphene nano-structure on top of Calcium fluoride (CaF_2) substrate with thickness of d = 20 nm of CaF_2. The periodicity of unit cell is fixed as 100 nm, and R1 = 40 nm, R2 = 10 nm and S = $20\sqrt{2}$ nm. Here, CaF_2 is selected as dielectric substrate due to its broadband transparency in the mid-infrared region and suitable dielectric properties [26]. The refractive index of CaF_2 is 1.43. Further, in order to modulate the Fermi level of graphene, the top gate technique is used here. The graphene Fermi level can be modulated in a wide range by this ion-gel top gating method. There are some papers using this method [27–30].

Optical Materials EXPRESS

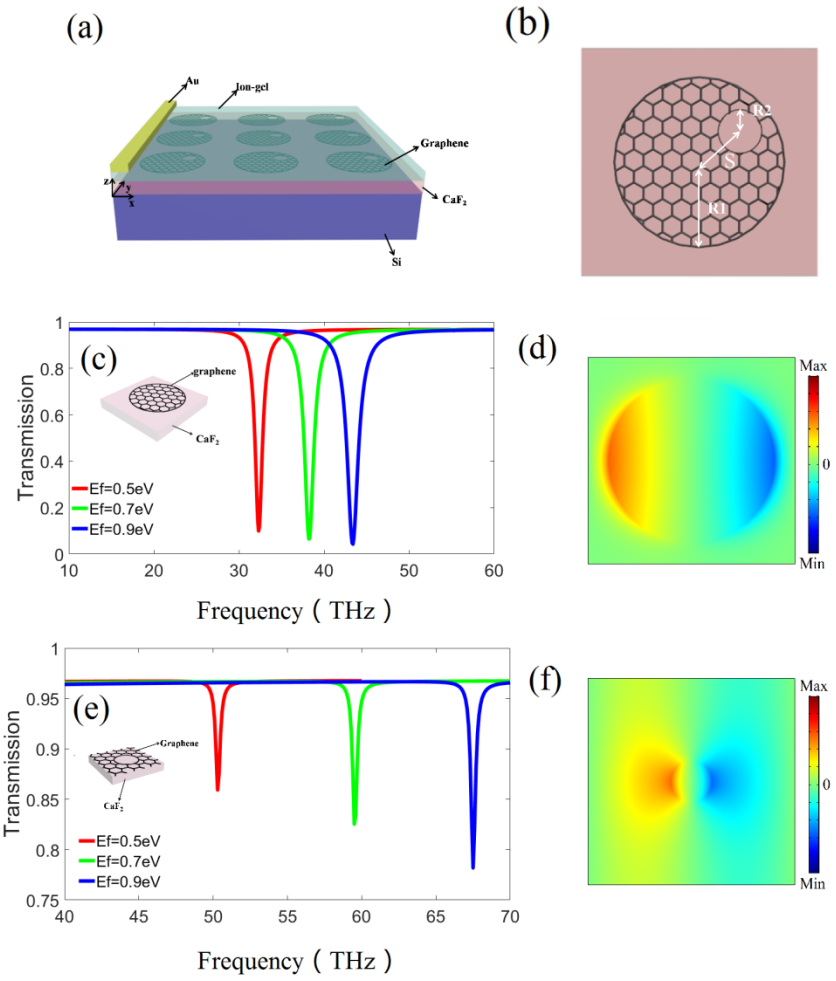

Fig. 1. (a) Schematic graph of the array of graphene nano-structure, which is fabricated on the CaF_2 layer. The ion-gel layer deposits was spin-coated on top of the graphene disk arrays to apply the bias voltage, and the Au gate contact deposited on the top. The Si layer is used to apply the gate voltage too. (b) The top view of the unit of the graphene structures. The periodicity of unit cell is fixed as 100 nm, where R1 = 40 nm, R2 = 10 nm and S = $20\sqrt{2}$ nm. (c) The transmission spectrum of graphene disk structure without circular defect. (d) The electric field distribution of z component of graphene disk. (e)The transmission spectrum of graphene layer with circular defect only. (f) The Electric field distribution of z component of circular defect.

In the mid-infrared region, the intraband conductivity term usually dominates over the interband term. Therefore, the interband transmission is negligible comparing to the intraband transmission in the mid-infrared range. Graphene's surface conductivity is well described by the Drude model and the equivalent relative permittivity is derived from the surface conductivity, as follows [15]:

$$\varepsilon_g = 1 + i\sigma / \varepsilon_0 \omega t_g \quad , \quad \sigma_g = \frac{e^2 E_f}{\pi \hbar^2} \cdot \frac{i}{\omega + i\tau^{-1}} \tag{1}$$

where e represents electron charge, ω is the angular frequency of the incident wave, $\hbar$ is the reduced Planck constant, E_f is the Fermi energy of the graphene layer, ε_0 is the permittivity of

Optical Materials EXPRESS

free space and the graphene layer thickness is t_g = 1 nm. The relaxation time is $\tau = \mu E_f / e v_f^2$, with Fermi velocity of $v_f = c/300$ and the carrier mobility of graphene $\mu = 10000\ cm^2 V^{-1} s^{-1}$.

In this work, the room temperature (T = 300 K) is assumed. The simulation is performed using commercial software COMSOL Multiphysics, based on the finite-element method, and the periodic boundary conditions are used in the xy plane; the Floquet ports are applied in the z direction. In the simulation, the electric field is polarized in the x direction.

The proposed defect graphene disk structure can be seen as an interaction between the plasmon responses of a graphene disk without circular defect and a circular defect [31]. Because of the finite spacing, the graphene plasmons arisen from the disks and circular defects interact with each other.

Figure 1(c) shows the transmission spectra of graphene disk without the circular defect at different Fermi levels. The radius of graphene disk is 40 nm. When the Fermi levels range from 0.5 to 0.9 eV, a dipolar resonance at 30-50 THz regime was found in the symmetric graphene disk structure, which can be confirmed in Fig. 1(d). The resonance frequency of the dipole mode excited in the individual graphene disk can determined via the equation [30,32,33]

$$\omega_p \approx \sqrt{\frac{2\alpha c L_1 E_f}{\pi\hbar(\varepsilon_1+\varepsilon_2)D}} \propto \sqrt{\frac{E_f}{D}} \tag{2}$$

where L_1 = 12.5, c is the speed of light in free space, $\alpha \approx 1/137$ is the fine-structure constant, ε_1 and ε_2 are the dielectric permittivities of the materials above and below the graphene disk, respectively, and D is the diameter of the graphene disk.

Figure 1(e) shows the transmission spectra of graphene layer with circular defects. The radius of the circular defect is 10 nm. A dipolar resonance at 50-70 THz regime was observed when changing the Fermi levels from 0.5 eV to 0.9 eV, which can also be confirmed in Fig. 1(f).

2.2 Numerical demonstrations of the dual-band resonance

The proposed graphene disk with circular defect structure utilizes the plasmon hybridization model, and excites high quality dual band resonances, as shown in Figs. 2(a)-2(f). Here, the Fermi level is 0.7 eV. It can be concluded from Figs. 2(a) and 2(b) that when the circular defect and the disk are concentric, the dipole resonance of the disk and the dipole resonance of the circular defect are excited. In this case, the disk dipole plasmon can interact with the plasmon of the circular defect, producing bonding (low-energy) and anti-bonding (high-energy) hybridized states. Due to the plasmon hybridization between the graphene disk and circular

Optical Materials EXPRESS

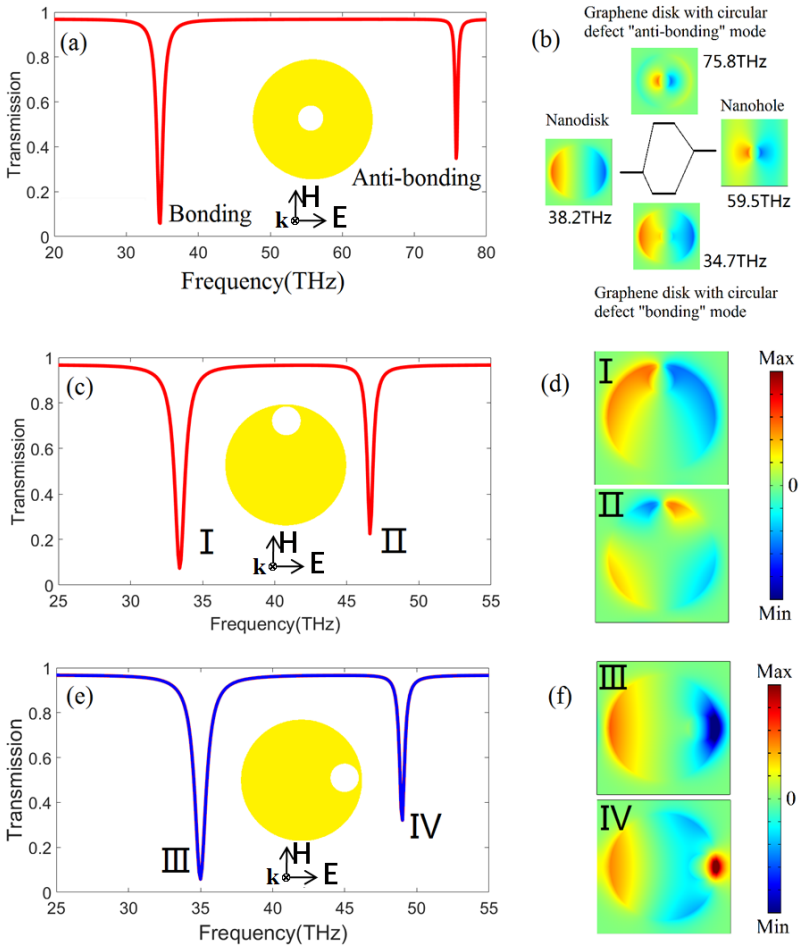

Fig. 2. Bonding and anti-bonding hybridized plasmons in graphene disk with circular defect under normal incidence. (a) Transmission spectra when graphene disk and circular defects are concentric. (b) Energy-level diagram to describe the plasmon hybridization effect in the proposed structure due to the mutual coupling between the graphene disk and circular defect. (c-d) Transmission spectra and electric field distribution when the circular defect is on the x-axis. (e-f) Transmission spectra and electric field distribution when the circular defect is on the y-axis. The illustrations are the schematic representation of the location of a circular defect in the graphene disk.

defect, the bonding (anti-bonding) mode is red (blue) shifted to 34.7 THz (75.8 THz), as compared to the dipole resonance frequency of the graphene disk (the circular defect), shown in Fig. 2(c) (Fig. 2(d)). The resonance frequencies of the bonding and anti-bonding modes can also be derived from Eq. (2). Here the values of L1 depend on the ratio of inner-to-outer diameters D_{defect}/D_{disk}, it can be find in Ref. 32. Such behaviors perfectly justify our idea to realize the dual-band resonance based on the plasmon hybridization model, as schematically shown in Fig. 3(b). Figures. 2(c) and 2(d) show the case where the circular defect is on the y-axis with a shift distance of $20\sqrt{2}$ nm. Compared with the case where the circular defect and the graphene disk are concentric, the resonance frequency of the bonding mode has a blue shift, and the resonance frequency of the anti-bonding mode has a red shift. The electric field distribution of the two modes can be observed from Fig. 2(d). Similarly, Figs. 2(e) and 2(f) show the case where the circular defect is on the x-axis with a shift distance of $20\sqrt{2}$ nm.

Optical Materials EXPRESS

Since the incident wave is x-polarized, the effect is different when the circular defect positions are different. The resonance frequencies of the two modes have blue shift compared to the case where the circular defect is on the y-axis. Figure 2(f) shows the electric field distribution of the two modes in this case.

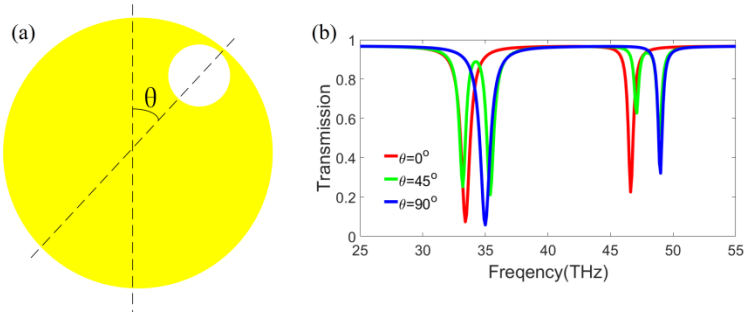

Fig. 3. (a) Schematic of the planar defect graphene structure with different offset angle θ. (b)Simulated transmission spectra of bonding mode and anti-bonding mode resonance with θ = 0°, 45° and 90°.

It can be observed from Figs. 2(a)-2(f) that when the circular defects are located at different positions of the graphene disk, the plasmon hybridization effect between them has different effects on the bonding and anti-bonding resonance. Therefore, the polarization selectivity of graphene disk with circular defect have been studied in this part. Here the radii of graphene disk and circular defect are 40 nm and 10 nm. The Fermi level is 0.7 eV. When the incident wave is x-polarized and the circular defect is on the y-axis (θ = 0°), the resonances of the bonding and anti-bonding modes are 33.4 THz and 44.6 THz, respectively, and the electric field distribution can be observed from Fig. 2(d). When the circular defect is on the x-axis (θ = 90°), the resonances of the bonding and anti-bonding modes are 35 THz and 49 THz, respectively, and the electric field distribution can be observed from Fig. 2(f). As the circular defect moves from the y-axis to the x-axis (θ = 0° to 90°), the transmission dips(both the bonding and anti-bonding modes) gradually changes from θ = 0° to θ = 90°. This can be verified from the transmission curve of θ = 0°, θ = 45° and θ = 90° in Fig. 3(b). These results indicate that circular defect with different offset angles on the graphene disk are polarization sensitive.

The influence of the Fermi level on the resonance spectra curves is shown in Fig. 4(a), taking the benefit of tunable surface conductivity by adjusting its Fermi energy. When the Fermi level is increased from 0.5 eV to 1.0 eV, the corresponding amplitude is almost unchanged, and the dual-band resonance peaks has a blue shift, realizing the modulation function in the interest frequency range, as shown in Fig. 4(a). Thus, by adjusting the Fermi level, dynamically controlled the dual-band resonance peaks are achieved without reconstructing the geometry or integrating metamaterials with other active components. Figure 4(b) shows the transmission spectral curves of the proposed structure with different circular defect radius, where the graphene disk radius is 40 nm, the defect shift distance is $20\sqrt{2}$ nm and the Fermi level is 0.7 eV. As R2 increases, the resonance amplitude of the transmission peaks are decreases, and the resonance frequency has a red shift.

Optical Materials EXPRESS

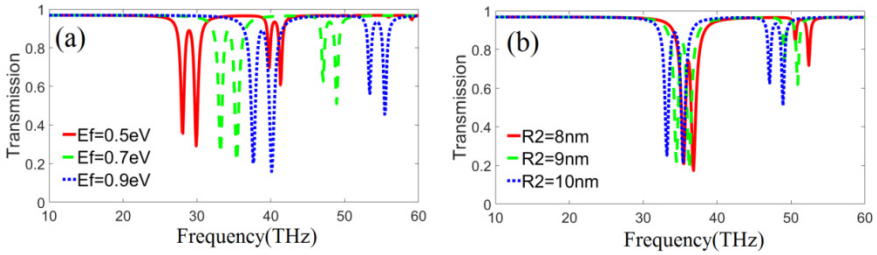

Fig. 4. (a) Transmission spectra at different Fermi levels with the values of 0.5, 0.7 and 0.9 eV. The graphene disk radius is 40nm, and the defect shift is $20\sqrt{2}$ nm. (b) Transmission spectra at different circular defect radius with the values of8 nm, 9 nm and 10 nm.

2.3 Refractive-index sensing performance of the defect graphene structure

In this part, the performance of the dual-band resonance peaks has been evaluated. Compared with the recent research, the proposed defect graphene disk structure is more sensitive [34]. Different refractive indices are set as analytes on the devices.

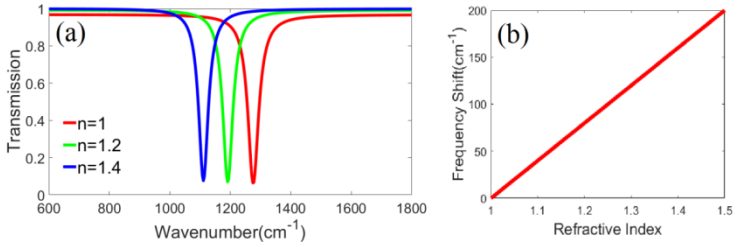

Fig. 5. (a) The transmission spectra of the graphene disk dipole resonance mode with different refractive indices. (b) Frequency shift of the dipole resonance mode versus the refractive index
.

Figure 5(a) shows the transmission spectra of the graphene disk structure with different refractive indices from 1 to 1.5. Here, the Fermi level is 0.7 eV. The dipole resonance dip frequency has a red shift (from 1274 cm^{-1} to 1111 cm^{-1}) as the refractive index increase from 1 to 1.4. Here, the wavenumber is defined as: $\tilde{\nu} = 1/\lambda$. Where λ is the wavelength [35]. The dipole resonance dip frequencies of the graphene disk are plotted together as a function of the refractive index, as shown in Fig. 5(b). There is a linear change in these frequency shifts, and the slopes of these lines are defined as the sensitivity (approximately 400 cm^{-1}/RIU). The ratio of the sensitivity to the FWHM of the resonance [(cm^{-1} /RIU)/FWHM] determines the FOM of metamaterials. The FOM value of the graphene disk structure is around 12.9.

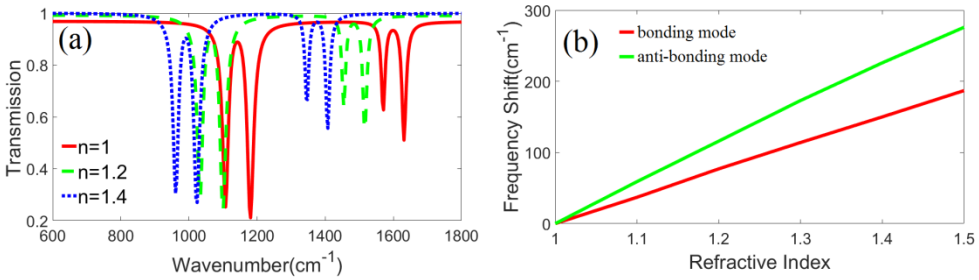

Fig. 6. (a) The transmission spectra of the defect graphene disk structure's dual-band resonances with different refractive indices. (b) Frequency shift of bonding mode and anti-bonding mode resonance peaks versus the refractive index.

Optical Materials EXPRESS

Compared with the graphene disk structure, the transmission spectra of the defect graphene disk structure's dual-band resonance curves with different refractive indices is shown in Fig. 6(a). Here, the graphene disk radius is 40 nm, the radius of the circular defect is 10 nm, $S = 20\sqrt{2}$ nm, $\theta = 45°$ and the Fermi level is 0.7 eV. The resonance peaks frequencies are plotted together as a function of the refractive index, as shown in Fig. 6(b). The sensitivities of the defect graphene structure are 370 and 550 cm^{-1}/RIU for the bonding and anti-bonding mode resonance peaks, respectively. This clearly reflects that the sensitivity of the sensor is enhanced by the anti-bonding mode resonance peak. We choose the sharp transparency peak and the higher dip (compared with two dips) on the resonances curve as two extreme points and then note the full-width at half-maximum bandwidth [36]. The FOM values of the bonding and anti-bonding mode resonance peaks are around 11 and 20.4, respectively.

3. Conclusion

In summary, the high-quality dual-band response has been demonstrated in an asymmetric defect graphene disk structure. When a circular defect is introduced in the graphene disk, the plasmon hybridization effect between them produces a dual-band resonance. The electric-field distributions and energy-level diagram explain the basic resonance mechanisms. The two excited response peaks have superior refractive-index sensing performance. The results demonstrate that the excited resonance can be modulated by the Fermi levels, the defect radius and the position of the defect. Compared with the normal graphene disk structure, the sensitivity and FOM of the dual-band resonance peaks are higher. In this work, the frequency sensitivity of the defect graphene disk structure is able to reach 550 cm^{-1}/RIU and the FOM value can reach 20.4. Therefore, the proposed defect graphene disk structure is a promising method for biosensing, gas detection and food safety etc. And the dual-band responses will help promote the development of multi-substance detection.

Funding

2016 Zhejiang Provincial Natural Science Foundation (Grant No.LY16F010010); 2015 Zhejiang Province Public Welfare of International Cooperation Project (Grant No. 2015C34006); 2013 National Natural Science Foundation of China under Grant No.61379027.

References

1. Y. Y. Xie, Y. X. Huang, W. L. Zhao, W. H. Xu, and C. He, "A Novel Plasmonic Sensor Based on Metal–Insulator–Metal Waveguide With Side-Coupled Hexagonal Cavity," IEEE Photonics J. **7**(2), 1–12 (2015).
2. A. Akhavan, H. Ghafoorifard, S. Abdolhosseini, and H. Habibiyan, "Plasmon-induced transparency based on a triangle cavity coupled with an ellipse-ring resonator," Appl. Opt. **56**(34), 9556–9563 (2017).
3. X. Yang, X. Hu, Z. Chai, C. Lu, H. Yang, and Q. Gong, "Tunable ultracompact chip-integrated multichannel filter based on plasmon-induced transparencies," Appl. Phys. Lett. **104**(22), 221114 (2014).
4. R. Li, D. Wu, Y. Liu, L. Yu, Z. Yu, and H. Ye, "Infrared Plasmonic Refractive Index Sensor with Ultra-High Figure of Merit Based on the Optimized All-Metal Grating," Nanoscale Res. Lett. **12**(1), 1 (2017).
5. B. C. Pan, Z. Liao, J. Zhao, and T. J. Cui, "Controlling rejections of spoof surface plasmon polaritons using metamaterial particles," Opt. Express **22**(11), 13940–13950 (2014).
6. C. Caucheteur, T. Guo, F. Liu, B. O. Guan, and J. Albert, "Ultrasensitive plasmonic sensing in air using optical fibre spectral combs," Nat. Commun. **7**, 13371 (2016).
7. J. Shibayama, K. Shimizu, J. Yamauchi, and H. Nakano, "Surface Plasmon Resonance Waveguide Sensor in the Terahertz Regime," J. Lightwave Technol. **34**(10), 2518–2525 (2016).
8. I. Alnaib, R. Singh, C. Rockstuhl, F. Lederer, S. Delprat, D. Rocheleau, M. Chaker, T. Ozaki, and R. Morandotti, "Excitation of a high-Q subradiant resonance mode in mirrored single-gap asymmetric split ring resonator terahertz metamaterials," Appl. Phys. Lett. **101**, 77–79 (2012).
9. A. V. Kabashin, P. Evans, S. Pastkovsky, W. Hendren, G. A. Wurtz, R. Atkinson, R. Pollard, V. A. Podolskiy, and A. V. Zayats, "Plasmonic nanorod metamaterials for biosensing," Nat. Mater. **8**(11), 867–871 (2009).
10. K. V. Sreekanth, Y. Alapan, M. ElKabbash, E. Ilker, M. Hinczewski, U. A. Gurkan, A. De Luca, and G. Strangi, "Extreme sensitivity biosensing platform based on hyperbolic metamaterials," Nat. Mater. **15**(6), 621–627 (2016).

Optical Materials EXPRESS

11. Z. Sekkat, S. Hayashi, D. V. Nesterenko, A. Rahmouni, S. Refki, H. Ishitobi, Y. Inouye, and S. Kawata, "Plasmonic coupled modes in metal-dielectric multilayer structures: Fano resonance and giant field enhancement," Opt. Express **24**(18), 20080–20088 (2016).
12. A. R. Wright and C. Zhang, "Dynamic conductivity of graphene with electron-LO-phonon interaction," Phys. Rev. B **81**, 165413 (2010).
13. A. N. Grigorenko, M. Polini, and K. S. Novoselov, "Graphene plasmonics," Nat. Photonics **6**(11), 749–758 (2012).
14. F. Xia, H. Wang, D. Xiao, M. Dubey, and A. Ramasubramaniam, "Two-dimensional material nanophotonics," Nat. Photonics **8**(12), 899–907 (2014).
15. F. J. G. D. Abajo, "Graphene Plasmonics: Challenges and Opportunities," ACS Photonics **1**, S2 (2014).
16. Z. Fei, A. S. Rodin, G. O. Andreev, W. Bao, A. S. McLeod, M. Wagner, L. M. Zhang, Z. Zhao, M. Thiemens, G. Dominguez, M. M. Fogler, A. H. Castro Neto, C. N. Lau, F. Keilmann, and D. N. Basov, "Gate-tuning of graphene plasmons revealed by infrared nano-imaging," Nature **487**(7405), 82–85 (2012).
17. J. Chen, M. Badioli, P. Alonso-González, S. Thongrattanasiri, F. Huth, J. Osmond, M. Spasenović, A. Centeno, A. Pesquera, P. Godignon, A. Z. Elorza, N. Camara, F. J. García de Abajo, R. Hillenbrand, and F. H. Koppens, "Optical nano-imaging of gate-tunable graphene plasmons," Nature **487**(7405), 77–81 (2012).
18. R. Zafar and M. Salim, "Enhanced Figure of Merit in Fano Resonance-Based Plasmonic Refractive Index Sensor," IEEE Sens. J. **15**(11), 6313–6317 (2015).
19. C. I. L. Justino, A. R. Gomes, A. C. Freitas, A. C. Duarte, and T. A. P. Rocha-Santos, "Graphene based sensors and biosensors," Trac Trends Anal. Chem. **91**, 53–66 (2017).
20. S. Kabiri Ameri, R. Ho, H. Jang, L. Tao, Y. Wang, L. Wang, D. M. Schnyer, D. Akinwande, and N. Lu, "Graphene Electronic Tattoo Sensors," ACS Nano **11**(8), 7634–7641 (2017).
21. J. Wang, C. Song, J. Hang, Z. D. Hu, and F. Zhang, "Tunable Fano resonance based on grating-coupled and graphene-based Otto configuration," Opt. Express **25**(20), 23880–23892 (2017).
22. X. He, F. Lin, F. Liu, and W. Shi, "Tunable high Q-factor terahertz complementary graphene metamaterial," Nanotechnology **29**(48), 485205 (2018).
23. X. He, P. Gao, and W. Shi, "A further comparison of graphene and thin metal layers for plasmonics," Nanoscale **8**(19), 10388–10397 (2016).
24. C. Sun, Z. Dong, J. Si, and X. Deng, "Independently tunable dual-band plasmonically induced transparency based on hybrid metal-graphene metamaterials at mid-infrared frequencies," Opt. Express **25**(2), 1242–1250 (2017).
25. Z. Dong, C. Sun, J. Si, and X. Deng, "Tunable polarization-independent plasmonically induced transparency based on metal-graphene metasurface," Opt. Express **25**(11), 12251–12259 (2017).
26. H. Hu, X. Yang, F. Zhai, D. Hu, R. Liu, K. Liu, Z. Sun, and Q. Dai, "Far-field nanoscale infrared spectroscopy of vibrational fingerprints of molecules with graphene plasmons," Nat. Commun. **7**, 12334 (2016).
27. X. He, F. Liu, F. Lin, and W. Shi, "Graphene patterns supported terahertz tunable plasmon induced transparency," Opt. Express **26**(8), 9931–9944 (2018).
28. N. Mou, S. Sun, H. Dong, S. Dong, Q. He, L. Zhou, and L. Zhang, "Hybridization-induced broadband terahertz wave absorption with graphene metasurfaces," Opt. Express **26**(9), 11728–11736 (2018).
29. J. H. Cho, J. Lee, Y. Xia, B. Kim, Y. He, M. J. Renn, T. P. Lodge, and C. D. Frisbie, "Printable ion-gel gate dielectrics for low-voltage polymer thin-film transistors on plastic," Nat. Mater. **7**(11), 900–906 (2008).
30. Z. Fang, Y. Wang, A. E. Schlather, Z. Liu, P. M. Ajayan, F. J. de Abajo, P. Nordlander, X. Zhu, and N. J. Halas, "Active tunable absorption enhancement with graphene nanodisk arrays," Nano Lett. **14**(1), 299–304 (2014).
31. E. Prodan, C. Radloff, N. J. Halas, and P. Nordlander, "A hybridization model for the plasmon response of complex nanostructures," Science **302**(5644), 419–422 (2003).
32. Z. Fang, S. Thongrattanasiri, A. Schlather, Z. Liu, L. Ma, Y. Wang, P. M. Ajayan, P. Nordlander, N. J. Halas, and F. J. García de Abajo, "Gated tunability and hybridization of localized plasmons in nanostructured graphene," ACS Nano **7**(3), 2388–2395 (2013).
33. Z. Fang, Y. Wang, A. E. Schlather, Z. Liu, P. M. Ajayan, F. J. de Abajo, P. Nordlander, X. Zhu, and N. J. Halas, "Active Tunable Absorption Enhancement with Graphene Nanodisk Arrays," Nano Lett. **14**(1), 299–304 (2014).
34. X. Guo, H. Hu, X. Zhu, X. Yang, and Q. Dai, "Higher order Fano graphene metamaterials for nanoscale optical sensing," Nanoscale **9**(39), 14998–15004 (2017).
35. H. Hu, X. Yang, F. Zhai, D. Hu, R. Liu, K. Liu, Z. Sun, and Q. Dai, "Far-field nanoscale infrared spectroscopy of vibrational fingerprints of molecules with graphene plasmons," Nat. Commun. **7**, 12334 (2016).
36. L. Chen, N. Xu, L. Singh, T. Cui, R. Singh, Y. Zhu, and W. Zhang, "Defect-Induced Fano Resonances in Corrugated Plasmonic Metamaterials," Adv. Opt. Mater. **5**(8), 1600960 (2017).

192.38.90.49 {ts '2018-12-05 04:22:59'}